ARTICLES

Femtosecond Dynamics of "TICT" State Formation in Small Clusters: The Dimethylaminobenzomethyl Ester−Acetonitrile System

G. Grégoire, I. Dimicoli, and M. Mons

DRECAM/SPAM, Bât. 522, CEA Saclay, 91911 Gif sur Yvette, France

C. Dedonder-Lardeux,* C. Jouvet, S. Martrenchard, and D. Solgadi

Laboratoire de Photophysique Moléculaire du CNRS, Bât. 210, Université de Paris-Sud, 91405 Orsay Cedex, France

Received: April 13, 1998; In Final Form: June 26, 1998

The solvent effect on the appearance of a red-shifted twisted intramolecular charge-transfer (TICT) emission is studied in molecular clusters. Using a supersonic expansion, dimethylaminobenzomethyl ester−acetonitrile (DMABME−$(CH_3CN)_n$) clusters are studied by monitoring at the same time mass spectra and dispersed fluorescence spectra as well as by lifetime measurements. For DMABME−$(CH_3CN)_n$ clusters, a clear red-shifted fluorescence is observed readily when the cluster contains one solvent molecule and the fluorescence decay becomes biexponential. Short-time evolution of the system has been monitored using a femtosecond pump/probe technique and picosecond photoelectron spectroscopy. The femtosecond dynamics is solvent dependent and is interpreted as a fast decay from the locally excited state to the TICT state reaching an equilibrium between these two states. The equilibrium shifts to the TICT states as the cluster size increases. The role of the triplet state in this process and in the biexponential character of the fluorescence is discussed.

Introduction

In this paper, we want to focus on solvent effects and particularly on the dynamics regarding the formation of "twisted intramolecular charge-transfer" (TICT) states, from the isolated molecule in the gas phase to solute/solvent clusters of increasing size. The TICT states are characterized by dual fluorescence[1] comprising a red-shifted fluorescence as compared to the normal fluorescence of the molecule in a nonpolar solvent. The concept of TICT states, first put forward by Grabowski et al.,[2−4] postulates the formation of an excited-state conformer of charge-transfer nature with near perpendicular arrangement regarding one single bond. It can be applied to quite a number of different solute families (for reviews see refs 3 and 5−8) ranging from aromatic amines, pyrroles, and carbazoles to biaryl compounds, the best known being 9,9′-bianthryl, and to charged species such as rhodamine or triphenylmethane dyes. The concept of TICT states finds its natural theoretical justification within the theory of biradicaloid states[9,10] and can also be applied to understand the polar solvent interaction on the excited-state twisting process of double bonds in substituted stilbenes.[8,11]

The necessity of a polar solvent is a natural consequence of the fact that TICT states are often higher in energy than the first excited state in the free molecule and can be populated only after sizable solvent stabilization, since charge-transfer states are more strongly stabilized than the other excited states due to a higher dipole moment.

The simplest molecule in which the TICT states are observed in a polar solvent is DMABN (dimethylaminobenzonitrile). Being the simplest molecule giving rise to a dual emission, it has been the subject of many theoretical calculations,[9−16] using different approaches (macroscopic, microscopic) to treat the solvent. In particular, the work of Kato and Amatatsu,[13] which takes into account the solvent effect through Molecular Dynamics simulations, suggests that the TICT state should be accessible in small water clusters.

Many attempts have been made to evidence the appearance of a TICT state in the DMABN molecule within polar clusters.[17−27] None was successful, which seems to indicate that the clusters are too cold to really solvate the molecule; in DMABN, the separation between the first excited state S_1 (L_b) and the S_2 (L_a) state, which correlates to the TICT state, is too large, so incomplete solvation does not stabilize this S_2 state enough to bring it below the S_1 (L_b) state.

In the dimethylaminobenzomethyl ester (DMABME) molecule, due to the stronger electron affinity of the methyl ester ($COOCH_3$) group as compared to the cyano group in DMABN, the S_2 state is lower in energy and the TICT state is already observed in the liquid phase in a weakly polar solvent (ref 5 and references therein). It has been shown that clustering of DMABME[25−27] with a few polar molecules leads to the observation of a red fluorescence, which has been assigned to the TICT-state emission.

In this paper, the early times of the dynamics, which leads to a red-shifted emission at the nanosecond time scale, have been studied by two methods.

(1) In picosecond photoelectron spectroscopy, the ionization potential should change with the geometry of the molecule, and

S1089-5639(98)01837-4 CCC: $15.00
Published on Web 09/19/1998

thus the dynamics of TICT formation should be reflected by the variation of the photoelectron spectrum.

(2) In size selected femtosecond resonant multiphoton ionization spectroscopy, during the geometry change, the ionization efficiency should change due either to the variation in the Franck−Condon factor between the excited state and the ionic state or to the change in the electronic character of the excited state. This will lead to a variation of the ion signal as the delay between the pump and the probe laser is changed.

The DMABME−CH_3CN system has been chosen because the absorption region (310−300 nm) of the clusters is well separated from the absorption of the free molecule, and therefore clusters can be excited without exciting the free molecule even with broad-band lasers such as a femtosecond source.

Experiment

Two experimental setups have been used. The setup in Orsay has been described previously; it consists of a supersonic beam coupled with a photoelectron or photoion time-of-flight spectrometer.[25] The frequency resolved fluorescence can be recorded at the same time as the mass spectrum is acquired. In this case, the laser is split into two beams. The first one crosses the supersonic expansion a few millimeters downstream from the nozzle, and the fluorescence is collected on the entrance slit of a monochromator (M 20 Jobin Yvon) set to a large bandwidth (5 nm). The second part of the laser is sent between the grids of the mass spectrometer to measure the cluster concentration. For lifetime measurements, a picosecond laser was used but the photomultiplier time response leads to a pulse width of 2.8 ns (fwhh).

For photoelectron spectra, the DMABME−$(CH_3CN)_n$ clusters are ionized either by resonant nanosecond two-photon absorption or with a 1 ps two-photon absorption.

The second apparatus in Saclay consists of a supersonic beam coupled with a time-of-flight mass spectrometer. In this experiment, pump and probe femtosecond lasers are used. The pump laser issued from a frequency-doubled dye laser ($\Delta t \approx$ 180 fs) at 305 nm excites the S_0-S_1 transition. Two probe wavelengths have been used; 395 nm is issued from the second harmonic of a titanium sapphire femtosecond laser, and 347 nm is obtained by mixing the first harmonic of the titanium sapphire laser with the first harmonic of the dye laser. No attempts have been made to recompress the pulse after mixing or doubling leading to a cross correlation of the lasers of 280 ± 20 fs measured in situ through the nonresonant ionization of NH_3.

Results

1. Fluorescence Lifetimes on a Nanosecond Time Scale. As we did for DMABME−water clusters,[25,26] we have repeated the experiment of Weersink and Wallace[27] on DMABME−CH_3CN but using a frequency resolved fluorescence detection, and the results obtained are in very good agreement with theirs. Fluorescence decays and mass spectra were recorded simultaneously to check that the one-to-one complex was the only complex observable in the jet.

For two observation wavelengths (330 and 410 nm), the fluorescence decays are biexponential; the preexponential factor as well as the time constants is found to be the same within experimental error (Figure 1).

The fluorescence lifetimes have been fitted using a biexponential decay: $I(t) = A_1 \exp(-t/T_1) + A_2 \exp(-t/T_2)$. The values for the different parameters used in the fit are listed in Table 1, together with the values of Weersink and Wallace.[27]

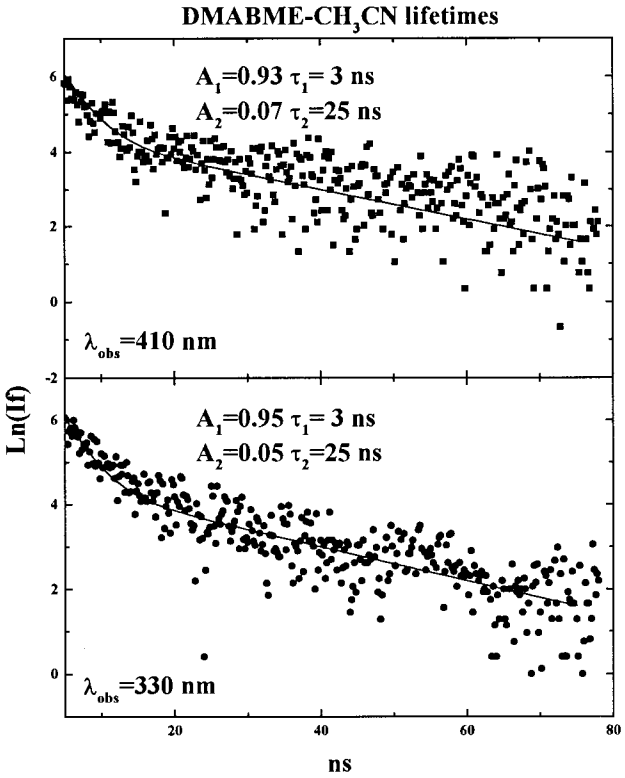

Figure 1. Fluorescence decays obtained after excitation of the DMABME−CH_3CN cluster at 305 nm. The fluorescence spectrum exhibits two distinct bands with maxima located at 330 and 410 nm, respectively. For both bands the fluorescence decay is biexponential and the lifetimes are similar to those reported by Weersink and Wallace.[27] The full lines represent the fit to the data obtained with the pre-exponential factors and time constants indicated in the figure.

TABLE 1: Pre-Exponential Factors and Time Constants Used To Fit the Fluorescence Decay

DMABME−CH_3CN	T_1 (ns)	T_2 (ns)	A_1	A_2
λ_{obs} 330 nm	3 ± 1	25 ± 5	0.95 ± 0.03	0.05 ± 0.03
λ_{obs} 410 nm	3 ± 1	25 ± 5	0.93 ± 0.03	0.07 ± 0.03
ref 27	4.5	40.9	0.9	0.1

The agreement between our experiment and that of Weersink and Wallace[27] is reasonable, taking into account that in both experiments the cluster concentration and temperature in the jet may not be exactly the same, and this also shows that the fluorescence decay times are not very sensitive to the cluster size, similar to the water case.[25,26] When the cluster size increases, the red/blue fluorescence ratio increases as in refs 25−27.

It should be mentioned that there is no observable rise time of the red emission associated with a similar decay of the blue emission, which would be expected in the case of a simple kinetic scheme where the S_1 state, responsible for the blue emission (330 nm), would decay into the 410-nm-emitting TICT state. The absence of a rise time for the red emission shows that if this red emission is the result of some dynamical process (TICT formation or solvent movement), this dynamical process is faster than the 2 ns resolution of the experiment and thus the decay observed in the blue and in the red band corresponds to an equilibrated mixed [S1(L_b)/TICT] state. Such a fast process should be evidenced by comparing the photoelectron spectra obtained with lasers having different temporal widths. The biexponential decay on the nanosecond time scale must then come from the coupling of the mixed state to another long-lived state.

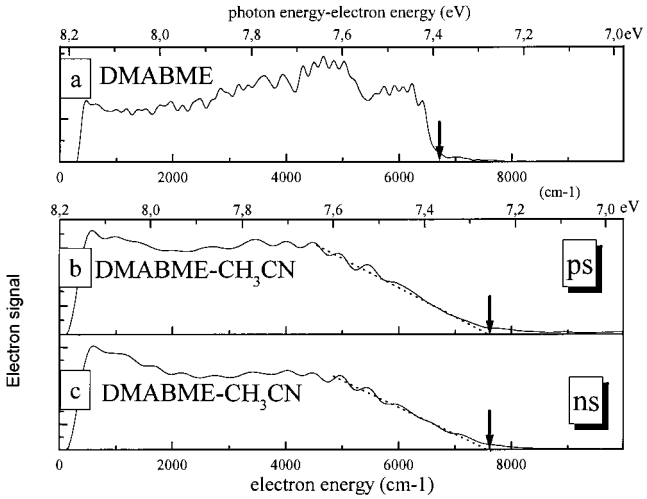

Figure 2. Photoelectron spectra (lower axis represents the photoelectron kinetic energy in wave numbers and upper axis represents the difference between total photon energy and electron energy in electron volts) of (a) free DMABME molecule excited at 301.6 nm (the most intense absorption band), (b) DMABME−CH_3CN complex excited with a 1 ps laser at 301.9 nm (only the clusters absorb at this wavelength), and (c) DMABME−CH_3CN complex excited with a 10 ns laser at 301.9 nm; no noticeable change between the picosecond and nanosecond photoelectron spectra can be evidenced. Broad arrows indicate the thresholds.

2. Photoelectron Spectra on the Nanosecond and Picosecond Time Scales. In Figure 2a is presented the photoelectron spectrum obtained when the free molecule is excited on the most intense absorption band process ($\lambda = 301.6$ nm) through a one-color two-photon absorption. The measured ionization threshold is in agreement with that reported in ref 26. In Figure 2 parts b and c, photoelectron spectra are recorded under similar jet-expansion conditions, with cluster sizes ranging from 1 to 5. The same one-color (301.9 nm) two-photon ionization scheme is used but with two temporal widths; Figure 2b is obtained with a 1 ± 0.3 ps laser, whereas the photoelectron spectrum 2c is obtained with a 10 ns pulse width. Within the experimental error the two spectra are the same.

The ionization threshold measured here for the complex is 7.25 ± 0.1 eV, which is lower than the mass-selected two-color two-photon ionization threshold measurement recorded on the DMABME−CH_3CN mass that gives 7.34 eV. But in the present experiment, not only the one-to-one complex but also larger clusters might be present in the expansion, which may explain this difference. Another element can account for the differences observed, namely the differences in the signal-to-noise ratio. Indeed, whatever the method, only a vertical ionization threshold is measured, and its determination depends crucially on the signal-to-noise ratio, which is certainly better in the photoelectron experiment than in the mass-selected two-color two-photon experiment where the two-color signal is always superimposed on a one-color signal, leading to a weaker detection efficiency and therefore to a higher value of the vertical threshold. In the two experiments, photoelectron spectrum and two-photon two-color ion threshold, there is no sharp onset of the signal as in the case of the free molecule. The electron or ion yield increases slowly with energy, which induces a rather large uncertainty on the threshold.

The similarity between nanosecond and picosecond spectra was not expected and will be explained in the light of the femtosecond experiments.

3. Femtosecond Pump/Probe Experiments. In these experiments, a first laser of 180 fs width at 305 nm excites selectively the $S_0 \rightarrow S_1$ transition of the DMABME−$(CH_3CN)_n$ clusters. The absorption spectrum of these clusters is known from previous work,[26,27] and at 305 nm (32 790 cm^{-1}, 4.06 eV) the excess energy in S_1 as compared to the onset of the absorption band is about 600 cm^{-1}. Two ionizing probe wavelengths have been used; with the first one at 347 nm (28 800 cm^{-1}, 3.57 eV) the total energy of the pump and probe photon (7.63 eV) is larger than the ionization threshold of the cluster, whereas the second probe wavelength used, 395 nm (25 300 cm^{-1}, 3.14 eV), leads to a total energy of 7.2 eV, smaller than the ionization threshold measured in nanosecond MPI experiments. At this energy, the photoelectrun spectrum shows that the one-photon ionization efficiency is very low; thus ionization with a 395 nm photon should be dominated by two-photon absorption.

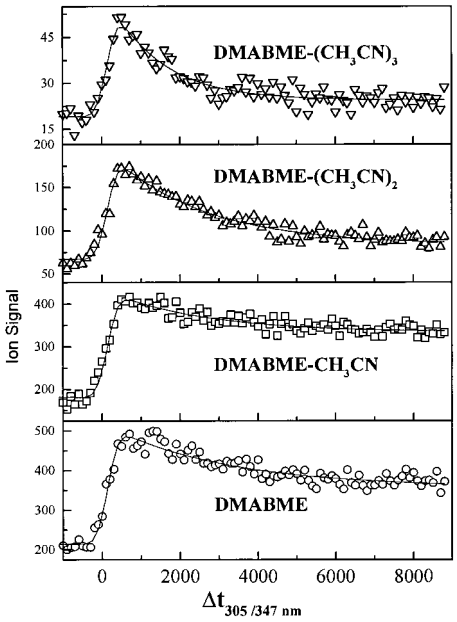

Figure 3. Time evolution of the ion signal as a function of the delay between the pump (305 nm) and the probe (347 nm) laser for different cluster sizes. The full lines are the fit obtained using eq 1 given in the text.

Figure 3 presents the time evolution of the DMABME−$(CH_3CN)_n$ ion signal as a function of the delay between the pump (305 ± 1 nm) and the probe laser (347 ± 1 nm) for different cluster sizes. The transients observed are different for each cluster size. They are characterized by a fast rise time, which is limited by the laser temporal width, a picosecond decay, and a plateau that is less important as the cluster size increases. The signal recorded on the free molecule mass is similar to the signal recorded at the mass of the one-to-one complex. Since the free molecule does not absorb[27] at the pump wavelength, the signal observed at this mass should come from the ionization of a larger cluster followed by the evaporation of a CH_3CN molecule in the ionic state.

The transients observed when the probe laser is set at 395 nm are presented in Figure 4. Surprisingly, as compared to Figure 3, the signal here increases when the delay between the pump and the probe laser increases. The signal changes with the cluster size; for small clusters an abrupt rise time corresponding to the laser temporal width is observed, whereas for larger ones the rise time is longer. The signal for the free molecule is similar to the one observed at 347 nm.

Discussion

Without going into the controversy[5,14,28] about which is the most important intramolecular coordinate responsible for the

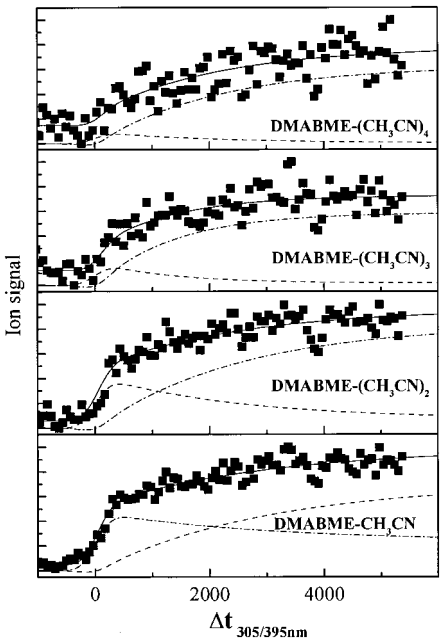

Figure 4. Time evolution of the ion signal as a function of the delay between the pump (305 nm) and the probe (395 nm) laser; curves in dashed lines represent $S_1(t)$ as calculated from eq 1, dot−dash curves represent TICT(t) calculated from eq 2, and the curves in full lines are the fit obtained using kinetic eq 3 explained in the text.

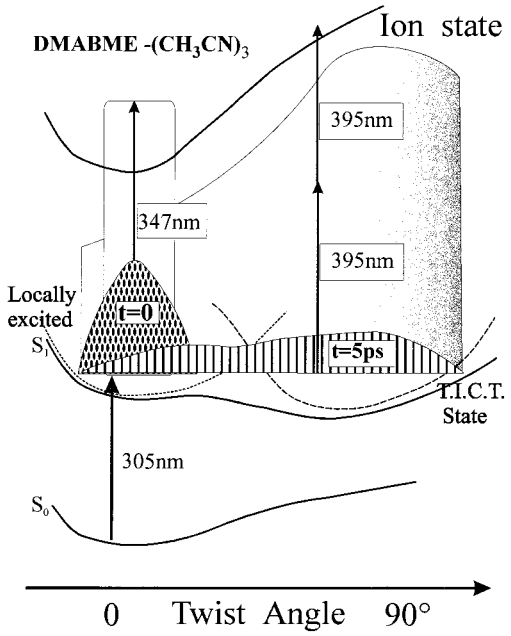

Figure 5. Scheme of the potential curves along the twist angle coordinate. At time $t = 0$ the femtosecond pulse prepares a wave packet (dark gray) at $\theta = 0°$, which diffuses to the TICT. After 5 ps, the wave packet is delocalized. This wave packet can be probed by a 347 nm photon in the vicinity of $\theta = 0°$ (vertically shaded gray). The 395 nm photon can probe the wave packet at different angles but more efficiently at $\theta = 90°$ (horizontally shaded gray).

appearance of a charge-transfer state induced by the solvent, we will discuss the results within the framework of the twisted intramolecular charge-transfer model. In the TICT representation, the following dynamical process is expected, assuming a two-dimensional reaction problem where one coordinate is the twist angle θ around the $C_{aryl}-N$ bond and the second is the solvent coordinate. The excitation photon prepares the locally excited S_1 state (L_b); in a concerted or sequential manner, the solvent molecules move to accommodate the new dipole moment of the excited state, which leads to a torsion of the molecule. A change in the ionization efficiency should be observed during this evolution from the locally excited state toward the TICT state, since the ionization threshold of the twisted molecule has no reason to be the same as the ionization threshold of the locally excited (untwisted) molecule. The ionization event is a different process in these two limiting cases; ionization of the L_b state corresponds to the removal of a π electron from the delocalized system comprising donor and acceptor, while ionization of the TICT state corresponds to the photodetachment of an electron from the negative moiety of the charge-transferred molecule.

The main points to be discussed concern the photoelectron spectra which stay identical in changing the time scale from 1 ps to 10 ns, while the femtosecond experiments reveal a dynamical process taking place on a few picosecond time scale as well as the long time behavior of the clusters observed in the biexponential fluorescence decays.

1. Photoelectron Spectra. The photoelectron spectra recorded using two-photon ionization with nanosecond or picosecond pulses are similar. One should thus conclude that there is no time evolution from the locally excited state to the TICT state.

If the TICT state is directly excited with the first photon, then the photoelectron spectrum is characteristic of the TICT state and will not change with the time scale. This is in contradiction with the femtosecond experiments, which clearly show an excited-state time evolution of a few picoseconds; this implies that the ionization efficiency changes with time and thus with the nature of the excited state.

Another possibility is that the ionization threshold does not change with the dynamics, i.e., the vertical ionization potential does not depend either on the twist angle or on the solvent coordinate. Once again, the femtosecond experiments that are probing through the ionic state show that the ionization efficiency is time dependent.

The explanation for the absence of an apparent evolution in the photoelectron spectra and the dynamics measured in the femtosecond experiments is given in the framework of the model depicted on Figure 5. Since the strong Coulomb interaction that leads to the stabilization of the TICT state in the neutral molecule has disappeared in the ion, a strong destabilization of the twisted configuration in the ion may be expected. Moreover, during the excited-state dynamics in going from the less stable locally excited state to the more stable TICT state (as pictured on Figure 5), from a classical point of view, a part of the potential energy is converted into kinetic energy during the molecular movement. As shown in small diatomic systems,[29] this kinetic energy must be conserved in the ionization process and therefore the effective ionization threshold at 90° will be higher than the vertical threshold. On the basis of the hypothesis of an ionic potential more stable around $\theta = 0°$ than at $\theta = 90°$, as shown on Figure 5, we assume that the ionization in the locally excited S_1 state is only efficient when the system is in a geometrical configuration which is close to that of the ground state (Franck−Condon approximation $\theta \approx 0°$), while the TICT state ($\theta \approx 90°$) does not ionize as easily. In this picture, the 1 ps experiment shows the $\theta \approx 0°$ Franck−Condon region before the evolution has started. In the nanosecond experiment, the wave packet is delocalized between locally excited and TICT states, but ionization around $\theta \approx 0°$ is always predominant; the photoelectron spectrum shows this $\theta \approx 0°$ Franck−Condon region.

2. Femtosecond Dynamics, Difference in Behavior for the Two Probe Wavelengths in the Femtosecond Experiment. Let us first point out some general features of any femtosecond experiment using as a probe the ionization of the excited state prepared by the pump photon. In such experiments, the dynamics of the excited state can be followed only if there is a strong evolution of the ionization efficiency when the dynamical process occurs. In the absence of such an evolution, the pump/probe signal recorded as a function of the delay between pump and probe pulses will lead to a step function. This has been clearly evidenced in diatomic molecules.[29] On the contrary, the observation of a time evolution of the ionic signal implies that the ionization efficiency changes during the evolution of the molecular movement in the initially prepared state.

As stated above, since the same pump photon is used and only the probe photon is changed, the same dynamical process is probed here with the two different probe wavelengths. The differences observed between Figures 3 and 4 reflect the differences of the ionization efficiencies.

For $\lambda = 347$ nm, as already stated, the photon energy is large enough to lead above the ionization threshold of the clusters. At this probe wavelength, the signal is maximized at $t = 0$, i.e., before any molecular rearrangement, and decays afterward in a few picoseconds; this implies that the locally excited state is efficiently ionized at 347 nm and the TICT state is not. This can also be deduced from the results obtained in the photoelectron experiment; the absence of evolution from picosecond to nanosecond implies that the TICT-state ionization efficiency is very low as compared to that of the locally excited state. As the cluster size increases the decay is faster, indicating that the TICT state is reached faster and more efficiently (see the kinetic model). After a few picoseconds, the signal is lower for larger clusters and this again corroborates the low ionization efficiency of the TICT state. It should be stressed that no oscillatory motion is observed, indicating that an equilibrium is reached quite quickly. The decay of the 347 nm signal probes the departure from the locally excited state to the TICT state.

At $\lambda = 395$ nm, the total photon energy is slightly below the measured ionization potential; thus, two photons are necessary to ionize the clusters. It is less obvious to understand which state is probed by this 395 nm photon. It is clear that a signal is observed at zero delay, which implies that the locally S_1 state may be ionized by this two-photon process. But a rise time on the order of 2 ps is also observed, close to the decay time obtained with a 347 nm photon; this means that with two 395 nm photons, ionization of the TICT state is more efficient than ionization of the S_1 state. This can be related to the appearance of a new absorption from the TICT state in the 400 nm spectral region observed in the DMABN molecule[30,31] in a polar liquid (CH_3CN for example). This band is similar to the anion absorption band[32,33] and has been ascribed to the anionlike absorption from the TICT state.

3. Kinetic Model. The results presented here can be fitted using a simple kinetic model similar to the one developed for the isomerization of *trans*-stilbene.[34]

The model is depicted in Figure 6. At time $t = 0$, the excitation promotes the system into the locally excited S_1 state (L_b); this state leads to an emission in the 330 nm region (rate constant k_{bf}) as for the free molecule. The locally excited state is coupled with a rate constant k_{12} to another state (state 2, which is assumed to be the TICT state). This process is reversible with a backward rate constant k_{21}. The TICT state leads to an emission in the 410 nm region (rate constant k_{rf}). To reproduce the biexponential fluorescence decay, it is necessary to add a third state (state 3), which is coupled to state 2 through a reversible process with rate constants k_{23} and k_{32}. This state, probably a triplet state as it will be discussed below, does not lead to any emission, and the rate constants involved are in the nanosecond range.

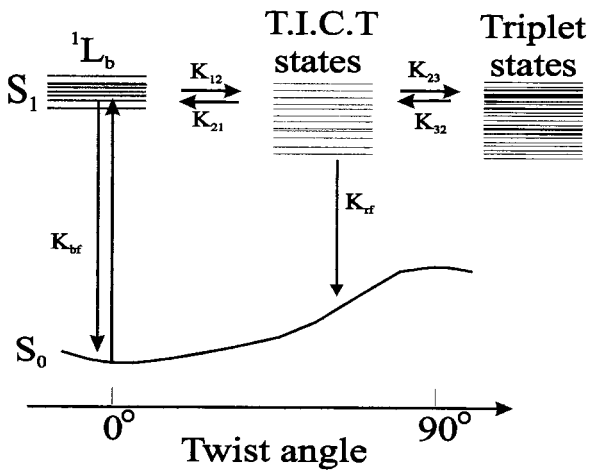

Figure 6. Kinetic model reproducing both the nanosecond and the femtosecond experiments with a set of time constants in agreement with the experimental observation for the DMABME−CH_3CN_1 complex; $1/k_{12} \approx 1/k_{21} \approx 6$ ps; $1/k_{23} \approx 2$ ns and $1/k_{32} \approx 10$ ns; and $1/k_{bf} \approx 5$ ns and $1/k_{rf} \approx 100$ ns.

TABLE 2: Evolution of the Kinetic Constants with the Cluster Size Using Eq 1

size n	$T_1 = 1/k_{12}$ (ps)	$T_2 = 1/k_{21}$ (ps)
0	6 ± 1	6 ± 1.5
1	6.5 ± 1	5 ± 1
2	3 ± 0.05	17 ± 4
3	1.5 ± 0.3	15 ± 5

Since the kinetics measured in the femtosecond experiment (on the order of a few picoseconds) is quite different from the kinetics observed in the nanosecond experiments, rate constants k_{12}, k_{21}, k_{23}, and k_{32} can be obtained separately. k_{12} and k_{21} are obtained from the femtosecond experiments while k_{23} and k_{32} are extracted from the fluorescence lifetimes.

Femtosecond Kinetics. The short-time behavior can be analyzed approximately without involving the nanosecond decay lifetimes ($1/k_{bf}$ and $1/k_{rf}$). The kinetic model is then

$$S_1 \underset{k_{12}}{\overset{k_{21}}{\rightleftharpoons}} \text{TICT}$$

The time evolution of the locally excited-state $S_1(t)$ is then given by

$$S_1(t) = \{k_{12} \exp(-(k_{12} + k_{21})t) + k_{21}\}/(k_{12} + k_{21})^1$$

The signal at long delay time, i.e., the height of the plateau, is given by the ratio $k_{21}/(k_{12} + k_{21})$. The time evolution of the TICT state is then

$$\text{TICT}(t) = \{1 - \exp(-(k_{12} + k_{21})t)\}\{k_{12}/(k_{12} + k_{21})\}^2$$

The experimental data have been fitted using this model, taking into account the temporal widths of the lasers. For the 347 nm probe laser, it has been assumed that only the S_1 state can be ionized and the results of the fit are given in Table 2.

From these values it clearly appears that:

(a) The rate constant k_{12} increases as the cluster size increases (the time necessary for the $S_1 \rightarrow$ TICT transition decreases as

the cluster size increases). The process is strongly reversible for small cluster sizes where the forward and backward rate constants are equal ($k_{12} \approx k_{21}$) and the equilibrium shifts toward the TICT state ($k_{12} > k_{21}$) when the cluster size increases.

(b) The time constants measured for the ion signal corresponding to the free molecule and to the one-to-one complex are very similar. Since the free molecule is not excited at 305 nm, the ion signal observed at this mass must come from the dissociation of the one-to-one complex in the ionic state.

The temporal evolution of the signal recorded when the probe laser is set at 395 nm has been modeled using the same kinetic model. The kinetic constants obtained from the fit of the 347 nm probe laser experiments have been used in the simulations. The difference between the two wavelengths is in the relative ionization efficiency of the TICT versus the S_1 state. The data have been fitted with the following (see Figure 4):

$$I_{395\ \mathrm{nm}}(t) = P_1\, \mathrm{S}_1(t) + P_2\, \mathrm{TICT}(t)^3$$

where the k_{ij} constants are taken from Table 2 and P_i represent the relative ionization efficiency. A very good agreement is obtained if the ratio P_2/P_1 is on the order of 3.0 ± 0.5 (see Figure 4), which implies an ionization efficiency of the TICT state 3 times greater than that of the S_1 state at 395 nm.

Nanosecond Fluorescence Lifetimes. The biexponential fluorescence lifetimes observed cannot be modeled unless a dark state coupled to the TICT state with time constants in the nanosecond range is included. We have seen above that the S_1 (L_b) state is in equilibrium with the TICT state, and on the nanosecond time scale, it can be considered that these states behave as a mixed state, which emits altogether in the blue (330 nm) and in the red (410 nm) regions.

Some reasonable assumptions have to be made in order to fit the data: the radiative lifetime of the L_b state is assumed to be the same in the cluster and in the free molecule, i.e., $1/k_{\mathrm{blue}} = 5$ ns; the dark state does not decay radiatively or at least not in the hundreds of nanosecond time domain; the rate constants k_{12} and k_{21} are the ones deduced from the femtosecond experiment.

A good agreement between the experimental data (Figure 1) and this kinetic scheme is obtained with the set of rate constants given in Figure 6.

With these assumptions, the total decay time of the TICT state can be deduced to be on the order of 100 ns, which is in agreement with the charge-transfer character of this state and the $1/k_{32}$ and $1/k_{32}$ time constants can be deduced to be in the nanosecond range, indicating that the coupling between the TICT state and the dark state is weak as compared to the coupling between the L_b state and the TICT state.

Evolution of the Kinetics with Cluster Size. It has already been seen that the emission of the TICT state increases, with respect to the resonant fluorescence, with the cluster size. This has been interpreted by an increasing stabilization of the TICT state as the cluster size increases. The evolution of the equilibrium between the L_b and the TICT states, i.e., the k_{12} and k_{21} rate constants, with the cluster size reflects the same process. Roughly speaking, the evolution of the rate constants is linked to the density of levels in both the L_b and TICT states.[34] In the one-to-one complex, $k_{12} \approx k_{21}$ and therefore the density of states should be similar in the L_b and TICT states. Since in the experiment the pump wavelength is set at 305 nm (32 790 cm^{-1}), the excess energy in the L_b state is (600 cm^{-1} (the absorption spectrum onset is 32 200 cm^{-1} in ref 27) and the excess energy in the TICT state should be similar, indicating that the L_b state and the TICT state lie at about the same energy in the one-to-one complex.

No direct measurement of the relative position of the L_b and L_a (which correlates to the TICT state) states has been done in the free molecule. It has been postulated that the L_a state is already below the L_b state in solution.[5] In the free molecule, the L_a state is slightly above the L_b state.[25] However, the interpretation of the kinetic measurement implies that the two states are quasidegenerate in the one-to-one complex and that only in larger complexes the TICT state is well below the L_b state as observed in the liquid phase.[5−25]

Role of the Triplet State. In the nanosecond fluorescence experiment, the biexponential decay observed in the DMABME−CH_3CN complex lifetime implies that the TICT state is coupled to a "dark state", which can be assigned to a triplet state. It should be noticed that in the free molecule as well as in the homodimer $DMABME_2$, the fluorescence decays are monoexponential. Evidence of the role of the triplet state induced by the TICT state has already been established in the case of DMABN in butanol by time-resolved infrared spectroscopy.[35] The intersystem crossing induced by the TICT state has been explained by Grabovsky et al.[3]—the TICT state can be considered as a diradical ion pair, formed of two doublet states. As a result of the perpendicular arrangement, the system decouples into two subsystems; the interaction between the two electrons on each radical should be small and therefore the ^{1}TICT and the ^{3}TICT states must be degenerate. In a classical time-dependent picture, when the system "oscillates" with a few picosecond "period" ($k_{12} \approx k_{21} \approx 6$ ps), between the TICT and the locally excited state, the spins are uncoupled in the TICT and are coupled in the L_b state. In the recoupling process, the spin may flip from the singlet to triplet every ≈1000 oscillations (number obtained from the ratio between the rate constants $k_{21}/k_{23} \approx 10^{-8}/10^{-11} \approx 10^3$).

In this simple interpretation, a biexponential decay would be expected for all charge-transfer processes as, for example, in the formation of exciplexes such as the one observed for the DMABME dimer.[25−27] In this case, the fluorescence consists of a red-shifted band (no locally excited emission) and the decay is purely monoexponential (35 ns). But in the simple picture described above, an equilibrium between the locally excited state and the CT state is necessary in order to see this spin-recoupling phenomenon. In the case of the $DMABME_2$, only one fluorescence band corresponding to the CT state is observed, which indicates an irreversible process from S_1 to the CT state, i.e., no spin recoupling and the presence of a triplet state is therefore not observed as a biexponential fluorescence decay.

Are the observed processes due to TICT, or can they be explained by the rearrangement of the solvent in an exciplex-type complex?

The conclusive evidence would have been the observation of recurrences at frequencies characteristic of the torsional motion. Since this has not been observed, one cannot bring strong evidence that the observed dynamics is due to the TICT state.

Maybe the coupling to the triplet state leading to the nanosecond biexponential decay is a better indication that a TICT state is involved. This seems to imply that the singlet and triplet states are quasidegenerate due to the very small interaction between the two electrons, which will be the case in the twisted configuration of the CT state. But it is not so clear for us that an exciplex-type complex could not exhibit such a small electron interaction.

Conclusions

The ultrafast dynamics observed in the formation of the TICT state in a finite system have shown that the rate of transfer from the locally excited state to the TICT state increases as the cluster size increases. Within a few picoseconds an equilibrium in the population of the locally excited and the charge-transfer states occurs. This equilibrium is shifted toward the TICT as the cluster size increases, reflecting the stepwise stabilization of the TICT state by the solvent molecules. As a result of the presence of an equilibrium between the locally excited and the TICT state, the singlet−triplet coupling can be observed in the biexponential decay of the fluorescence.

Acknowledgment. The authors are highly indebted to M. Meynadier, M. Perdrix, and S. Guizard for providing the femtosecond lasers. We also thank J.T. Hynes, Ph. Millié, and A. Tramer for helpful discussions.

References and Notes

(1) Lippert, E.; Lüder, W.; Boos, H. In *Advances in Molecular Spectroscopy*; Mangini, A., Ed.; Pergamon Press: Oxford, 1962; p 443.
(2) Rotkiewicz, K.; Grellmann, K. H.; Grabowski, Z. R. *Chem. Phys. Lett.* **1973**, *19*, 315; **1973**, *21*, 212.
(3) Grabowski, Z. R.; Rotkiewicz, K.; Siemiarczuk, A.; Cowley, D. J.; Baumann, W. *Nouv. J. Chim.* **1979**, *3*, 443.
(4) Grabowski, Z. R.; Rotkiewicz, K.; Siemiarczuk, A. *Lumin J.* **1979**, *18/19*, 420.
(5) Rettig, W. *Angew. Chem., Int. Ed. Engl.* **1986**, *25*, 971.
(6) Lippert, E.; Rettig, W.; Bonacic-Koutecký, V.; Heisel, F.; Miehé, J. A. *Adv. Chem. Phys.* **1987**, *68*, 1.
(7) Rettig, W. In *Modern Models of Bonding and Delocalization*; Liebman, J., Greenberg, A., Ed.; VCH Publishers: New York, 1988; Chapter 5, p 229.
(8) Rettig, W. In Electron Transfer I; *Topics in Current Chemistry*; Mattay, J., Ed.; Springer-Verlag: Berlin, 1994; Vol. 169, p 253.
(9) Michl, J.; Bonacic-Koutecký, V. *Electronic Aspects of Organic Photochemistry*; J. Wiley & Sons: New York, 1990.
(10) Bonacic-Koutecký, V.; Michl, J. *J. Am. Chem. Soc.* **1985**, *107*, 1765.
(11) Salem, L.; Rowland, C. *Angew. Chem., Int. Ed. Engl.* **1972**, *11*, 92.
(12) Rettig, W.; Majenz, W. *Chem. Phys. Lett.* **1989**, *154*, 335.
(13) Kato, S.; Amatatsu, Y. *J. Chem. Phys.* **1990**, *92*, 7241.
(14) Marguet, S.; Mialocq, J. C.; Millie, P.; Berthier, G.; Momicchioli, F. *Chem. Phys.* **1992**, *160*, 265.
(15) Andres, L. S.; Merchan, M.; Ross, B. O.; Lindh, R. *J. Am. Chem. Soc.* **1995**, *117*, 3189.
(16) Kim, H. J.; Hynes, J. T. *J. Photochem. Photobiol.* **1997**, *105*, 337.
(17) August, J.; Palmer, T. F.; Simons, J. P.; Jouvet, C.; Rettig, W. *Chem. Phys. Lett.* **1988**, *145*, 273.
(18) Kobayashi, T.; Futakami, M.; Kajimoto, O. *Chem. Phys. Lett.* **1986**, *130*, 63.
(19) Peng, L. W.; Dantus, M.; Zewail, A. H.; Kemnitz, K.; Hicks, J. M.; Eisenthal, K. B. *J. Phys. Chem.* **1987**, *91*, 6162.
(20) Gibson, E. M.; Jones, A. C.; Phillips, D. *Chem. Phys. Lett.* **1987**, *136*, 454.
(21) Warren, J. A.; Bernstein, E. R.; Seeman, J. I. *J. Chem. Phys.* **1988**, *88*, 871.
(22) Shang, Q.; Bernstein, E. R. *J. Chem. Phys.* **1992**, *97*, 60.
(23) Bernstein, E. R. *J. Phys. Chem.* **1992**, *96*, 10105.
(24) Grassian, V. H.; Warren, J. A.; Bernstein, E. R.; Secor, H. V. *J. Chem. Phys.* **1989**, *90*, 3994.
(25) Dedonder-Lardeux, C.; Jouvet, C.; Martrenchard, S.; Solgadi, D.; McCombie, J.; Howells, B. D.; Palmer, T. F.; Subaric, A.; Monte, C.; Rettig, W.; Zimmermann, P. *Chem. Phys.* **1995**, *191*, 271.
(26) Dedonder-Lardeux, C.; Martrenchard-Barra, S.; Jouvet, C.; Solgadi, D.; Krim, L.; Rettig, W.; Castano, F. *J. Chim. Phys.* **1995**, *62*, 465.
(27) Weersink, R. A.; Wallace, S. C. *J. Chem. Phys.* **1994**, *98*, 10710.
(28) Zachariasse, K. A.; von der Haar, T.; Hebecker, A.; Leinhos, U.; Kühnle, W. *Pure Appl. Chem.* **1993**, *65*, 1745.
(29) Jouvet, C.; Martrenchard, S.; Solgadi, D.; Dedonder-Lardeux, C.; Mons, M.; Grégoire, G.; Dimicoli, I.; Piuzzi, F.; Visticot, J. P.; Mestdagh, J. M.; D′Oliveira, P.; Meynadier, P.; Perdrix, M. *J. Phys. Chem. A* **1997**, *101*, 2555.
(30) Okada, T.; Mataga, N.; Baumann, W. *J. Phys. Chem.* **1987**, *91*, 760.
(31) Rullière, C.; Grabowski, Z. R.; Dobkowski, J. *Chem. Phys. Lett.* **1987**, *137*, 408.
(32) Chutny, B.; Swallow, A. J. *Trans. Faraday Soc.* **1970**, *66*, 2847.
(33) Shida, T.; Iwata, S.; Imamura, M. *J. Phys. Chem.* **1974**, *78*, 741.
(34) Syage, J. A.; Felker, P. M.; Zewail, A. H. *J. Chem. Phys.* **1984**, *81*, 4706.
(35) Hashimoto, M.; Hamaguchi, H. *J. Phys. Chem.* **1995**, *99*, 7875.